A&A 375, 739–751 (2001)
DOI: 10.1051/0004-6361:20010675

Astronomy & Astrophysics

Hard X–ray properties of blazars⋆

D. Donato[1], G. Ghisellini[1], G. Tagliaferri[1], and G. Fossati[2]

[1] Osservatorio Astronomico di Brera, Via Bianchi 46, 23807 Merate, Italy
[2] Center for Astrophysics and Space Sciences, University of California at San Diego, 9500 Gilman Drive, La Jolla, CA 92093-0424, USA

Received 16 February 2001 / Accepted 3 May 2001

Abstract. We have considered all blazars observed in the X–ray band and for which the slope of the X–ray spectrum is available. We have collected 421 spectra of 268 blazars, including 12 archival unpublished ASCA spectra of 7 blazars whose analysis is presented here. The X–ray spectra of blazars show trends as a function of their power, confirming that the blazar overall energy distribution can be parameterized on the basis of one parameter only, i.e. the bolometric luminosity. This is confirmed by the relatively new hard (2–10 keV) X–ray data. Our results confirm the idea that in low power objects the X–ray emission mechanism is the synchrotron process, dominating both the soft and the hard X–ray emissions. Low energy peaked BL Lac objects are intermediate, often showing harder spectra in the hard X–ray band, suggesting that the synchrotron process dominates in the soft band, with the inverse Compton process dominating at high energies. The most powerful objects have X–ray spectra that are flat both in the soft and in the hard band, consistent with a dominating inverse Compton component.

Key words. BL Lacertae objects: general – X–rays: galaxies

1. Introduction

Thanks to γ–ray observations of EGRET, on board CGRO, we now know the overall spectral energy distribution (SED) of blazars. They are characterized, in ν–$\nu F(\nu)$ plots, by two broad peaks. It is believed that the first, located in the IR–soft X–ray band, is due to synchrotron emission, while the second is due to the inverse Compton process by the same electrons producing the synchrotron part of the spectrum (Maraschi 1992; Sikora et al. 1994; but see Mannheim 1993 for a different interpretation). The 0.1–10 keV emission of blazars is therefore located in the minimum between the two peaks, where both processes (synchrotron and inverse Compton) can contribute. Observations in this band are therefore useful to characterize the relative importance of both processes. This can constrain models, allowing a better determination of the location of both peaks. Usually, a steep power law energy distribution in the X–ray band (with a spectral energy index $\alpha > 1$, with $F \propto \nu^{-\alpha}$) is due to the tail of the synchrotron spectrum, while $\alpha < 1$ flags the dominance of the inverse Compton spectrum. There are exceptions to this rule, such as HBL (High energy peaked BL Lacs) in a flaring state, which show a synchrotron spectrum peaking above 10 keV. One dramatic example of this behavior is Mkn 501, whose synchrotron peak energy, usually located below/at $\simeq$1 keV, shifted to 100 keV or more during its flare in April 1997 (Pian et al. 1998). In these cases the X–ray spectrum, usually steep during quiescence, becomes much flatter during flares.

Fossati et al. (1998) (F98 hereafter) have shown that blazars form a sequence, with their SED changing in a continuous way as their bolometric power changes: low luminosity objects (HBL) have the synchrotron peak in the UV–soft X–ray band, and the inverse Compton peak between the GeV and the TeV band. The two components have approximately the same power. As the bolometric luminosity increases, both peaks shift to lower frequencies, and the Compton peak becomes increasingly dominant. This trend offers the opportunity to unify in a single scheme the many flavors of existing blazars, and calls for a physical explanation (see e.g. Ghisellini et al. 1998).

To check the reliability of this trend we have collected data for all blazars having available spectral information in the X–ray band. For the soft band [0.1–2 keV], most of the results come from *ROSAT*, while for the 2–10 keV band the results are gathered from the EXOSAT, ASCA and *Beppo*SAX satellites.

Besides the data already published, we searched for unpublished data in the ASCA public archive, finding 12 observations of 7 sources. Results of the analysis of

Send offprint requests to: G. Ghisellini,
e-mail: Gabriele@merate.mi.astro.it

⋆ Table 5 is only available in electronic form at http://www.edpsciences.org

these data are presented here. We then add these sources to our sample.

The entire sample forms the largest database in the X–ray range: 421 spectra of 268 blazars. The X–ray data have been complemented by additional information regarding the redshift (when available), the radio flux at 5 GHz and the optical flux (in the V band).

The paper is organized as follows; Sect. 2 is devoted to the analysis of the 12 ASCA spectra, while in Sect. 3 we present the entire set of data. In Sect. 4 we compare the results in the soft and the hard X–ray bands and check for correlations with other spectral parameters, such as the broad band spectral indices connecting the radio with the optical fluxes, the optical with the X–ray fluxes, and the radio with the X–ray fluxes. In Sect. 5 we discuss our findings in the framework of the scenario proposed by Fossati et al. (1998), suggesting an improvement connected to a possible physical difference between low and high power sources.

2. Analysis of ASCA data

We searched the ASCA public archive at HEASARC, finding 12 observations of 7 blazars that have not been analyzed and published before: 0405–123 and PKS 0420–014 (classified as Flat Spectrum Radio Quasars, FSRQs); B2 1308+326 and 1807+698 (classified as Low Peaked BL Lac objects, LBLs); 1ES 1028+511, 1553+511 and 1ES 2344+514 (classified as High Peaked BL Lac objects, HBLs).

1ES 1028+511 and 1ES 2344+514 have 3 separate observations each, while B2 1308+326 was observed twice. The search for unpublished observations is updated to November 1999. During the preparation of this work the "Tartarus" data base became available[1], presenting results of an automatic spectral and temporal analysis for the AGNs observed by ASCA.

2.1. Data reduction and spectral analysis

We extracted the spectra of all sources from the files produced by the Revision–2 data release and included data transmitted in all 3 modes (High, Medium and Low) to increase the signal/noise ratio. The event files are obtained from all four instruments on board ASCA: the Solid–State Imaging Spectrometers (SIS0 and SIS1) and the Gas Imaging Spectrometers (GIS2 and GIS3). For the SIS we used the event files converted into BRIGHT mode. For a description of the ASCA observatory see e.g. Tanaka et al. (1994).

To screen the SIS and GIS data we follow the criteria given in the *ABC ASCA reduction guide*, rejecting the data taken during the passage of the South Atlantic Anomaly, or with geomagnetic cutoff rigidity lower than 8 GeV/c, or with angles between the targets and the day/night terminator smaller than 20° or for Elevation angles smaller than 5°.

The source spectra were extracted from circular regions centered on the sources, with radii of 6 arcmin for the GIS and 4 arcmin for the SIS0, while for the SIS1 the source is normally nearer to the detector border and we had to use a smaller radius of ∼3.3 arcmin. For the GIS we extracted the background in circular regions with the same dimensions used for the sources but centered on a symmetric point with respect to the optical axis, where the contribution of the source to the counts was negligible. For the SIS, instead, the background was extracted from blank field files because the sources occupied a large area of the detector. On these blank fields we chose circular regions with the same radii and positions used for the sources.

For the GIS spectra we used the 1994 May response matrices, while for the SIS spectra we generated the matrices with the SISRMG program of the FTOOLS V3.6 package. The ARF files for both SIS and GIS were derived with the ASCAARF V2.62 program. The GIS and SIS data were fitted in the channel ranges 69–1020 and 15–510, corresponding to the energy ranges 0.7–10 and 0.4–10 keV, respectively. The spectra were rebinned in order to have at least 25 counts in each new bin.

The ASCA spectra were fitted using XSPEC V10 with four models: single or broken power law with free or fixed (Galactic) absorption. The cross section for photoelectric absorption is calculated following Morrison & McCammon (1983), while the Galactic column density in the direction of the sources was estimated from the 21 cm radio maps of neutral hydrogen (Brinkmann & Siebert 1994; Danly et al. 1992; Dickey & Lockman 1990; Elvis et al. 1989; Lamer et al. 1996; Lockman & Savage 1995; Murphy et al. 1996). The data were fitted simultaneously from all the instruments with the same model. However, the normalizations were left as independent parameters for each data set to account for the cross–calibration uncertainties between the four detectors, estimated to be of the order of 6%. The differences found between the various normalizations were always consistent with these uncertainties.

2.2. Results of the fits

The results of the 12 spectral fits of the 7 blazars observed by ASCA are reported in Table 1. The uncertainties for the spectral parameters are at the 90% confidence errors for two parameters of interest ($\Delta\chi^2 = 4.6$). The unabsorbed integrated 2–10 keV and monochromatic 1 keV fluxes are obtained using only the SIS0 data. As the observations presented in this paper were all taken after 1994, they are most likely affected by the so-called "excess $N_{\rm H}$" problem. This is due to a degradation of the SIS efficiency below 1 keV which can give incorrect results for the column density and/or other parameters. As suggested in the ASCA Web site, to avoid the calibration uncertainties we considered only the SIS data above 1 keV in the SIS+GIS

[1] at `http://tartarus.gsfc.nasa.gov/`

Table 1. Best fits of the 12 observations. [a] day/month/year; [b] 10^{-12} erg cm^{-2} s^{-1}.

Source	Obs. date[a]	$N_{\rm H}$ 10^{21} cm^{-2}	Γ	$\chi^2_{\rm r}$/d.o.f.	$F^b_{[2-10]}$	$F_{1\,\rm keV}$ μJy
0405−123	09/08/1998	$0.72^{+0.51}_{-0.63}$	$1.76^{+0.09}_{-0.10}$	1.0/160	5.2	0.9
0420−014	31/08/1997	$0.90^{+1.04}_{-0.81}$	$1.86^{+0.19}_{-0.18}$	0.8/73	1.4	0.3
1028+511	28/04/1995	$1.01^{+0.23}_{-0.21}$	$2.53^{+0.06}_{-0.05}$	1.0/287	6.2	3.4
	29/04/1995	$1.33^{+0.18}_{-0.17}$	$2.59^{+0.05}_{-0.05}$	0.9/310	7.4	4.5
	08/05/1995	$1.12^{+0.12}_{-0.12}$	$2.49^{+0.04}_{-0.04}$	0.9/201	7.8	4.1
1308+326	10/06/1996	$1.97^{+2.96}_{-1.97}$	$1.99^{+0.47}_{-0.36}$	1.5/29	0.5	0.1
	11/06/1996	$0.97^{+1.01}_{-0.97}$	$1.74^{+0.32}_{-0.23}$	1.4/78	0.6	0.1
1553+113	16/08/1995	$1.30^{+0.62}_{-0.61}$	$2.47^{+0.19}_{-0.18}$	1.3/294	29.4	14.9
1807+698	05/11/1996	$0.50^{+0.28}_{-0.27}$	$1.75^{+0.07}_{-0.06}$	1.0/122	3.1	0.5
2344+514	10/01/1997	$2.71^{+0.17}_{-0.17}$	$2.13^{+0.03}_{-0.03}$	1.1/216	17.2	5.3
	23/01/1997	$2.91^{+0.34}_{-0.33}$	$2.39^{+0.08}_{-0.06}$	0.9/72	10.4	5.2
	10/12/1997	$2.93^{+0.37}_{-0.35}$	$2.31^{+0.07}_{-0.07}$	1.2/202	10.4	4.2

combined fit. Of the four models considered, according to the F–test, the one that better represents the data in all twelve cases is the single power law with free $N_{\rm H}$. In some cases (detailed below) we obtain a value for the absorbing column greater (by a factor 3–10) than the Galactic value. Note that the results obtained by the automatic analysis presented in the "Tartarus" database are in excellent agreement with ours (not surprisingly, since the same model is adopted). What is somewhat surprising is that the broken power law model (either with free or fixed $N_{\rm H}$) did not significantly improve the fits. This may be indicative of true extra–absorption or a spectral behavior more complex than those here examined (one possibility being a gradual but continuous steepening of the spectrum).

In the following we will compare the spectral properties of blazars in the soft and hard X–ray bands considering only the single power law model. To this end, the results of this model allow a more uniform comparison.

The results of spectral fit for the 7 sources are discussed below, grouped in the three subclasses (FSRQ, LBL and HBL).

2.2.1. FSRQ

For 0405–123, the best fit gives a flat photon spectral index $\Gamma = 1.76 \pm 0.1$, indicating the dominance of the inverse Compton component. The derived $N_{\rm H}$ value is consistent with the Galactic value, $N_{\rm H}^{\rm Gal} = 0.37 \times 10^{21}$ cm^{-2} (Danly et al. 1992).

Similar results are obtained for PKS 0420–014, with a photon spectral index $\Gamma = 1.86 \pm 0.19$. Also in this case the $N_{\rm H}$ value is consistent with the Galactic one ($N_{\rm H}^{\rm Gal} = 0.94 \times 10^{21}$ cm^{-2}, Elvis et al. 1989).

2.2.2. LBL

For B2 1308+326 there are two observations on two consecutive days. The spectra are quite noisy and also the reduced $\chi^2_{\rm r}$ are not very good. In both cases the best fits are obtained with a spectral index $\Gamma \simeq 1.75$–2.0. Due to the large error bars (see Table 1), the derived absorption column density can be consistent with the Galactic one ($N_{\rm H}^{\rm Gal} = 0.11 \times 10^{21}$ cm^{-2}, Lockman & Savage 1995).

For 1807+698 we obtained $\Gamma = 1.75 \pm 0.07$ and a value of $N_{\rm H}$ consistent with the Galactic one ($N_{\rm H}^{\rm Gal} = 0.44 \times 10^{21}$ cm^{-2}, Murphy et al. 1996).

2.2.3. HBL

1ES 1028+511 has been observed three times over a time span of two weeks. The source did not significantly vary in flux nor in shape ($\Delta\Gamma \simeq 0.12$). In all cases the best fits are obtained for a value of $N_{\rm H}$ a factor 10 larger than the Galactic one ($N_{\rm H}^{\rm Gal} = 0.12 \times 10^{21}$ cm^{-2}; Lamer et al. 1996).

For 1553+113 the best fit is obtained with a value of $N_{\rm H} \sim 3$ times larger than the Galactic one ($N_{\rm H}^{\rm Gal} = 0.37 \times 10^{21}$ cm^{-2}; Brinkmann & Siebert 1994).

The source 1ES 2344+514 has been observed three times, twice in Jan. 1997 and one in Dec. 1997. Both the fluxes and the spectral indices show some variability. The best fit value for the $N_{\rm H}$ is about 1.5 times the Galactic value ($N_{\rm H}^{\rm Gal} = 1.67 \times 10^{21}$ cm^{-2} Dickey & Lockman 1990).

3. The catalogue

3.1. Starting samples

Our purpose is to have the most complete ensemble of spectral information (fluxes and spectral indices) in the X–ray band, from 0.1 to 10 keV, of all known blazars. We therefore considered all blazars detected in the X–ray band, for which also a measure of the X–ray spectral index is available. We collected the data obtained by five X–ray satellites: *Einstein*, EXOSAT, *ROSAT*, ASCA and *Beppo*SAX (see Table 2).

The first step was to recognize if a source belongs to the blazar class, and to which subclass (i.e. if a source is a FSRQ or an HBL or an LBL). We used several published lists of blazars and other publications describing single recognized sources. We considered the Slew Survey Sample (Elvis et al. 1992; Perlman et al. 1996), the 2 Jy sample of Wall & Peacock (1985), and the 1 Jy BL Lac sample (Stickel et al. 1991). In addition, we used the lists taken from the works of Bade et al. (1994); Bade et al. (1998); Brinkmann et al. (1994); Brinkmann et al. (1997); Cappi et al. (1997); Comastri et al. (1997); Ghisellini et al. (1993); Lamer et al. (1996); Laurent–Muehleisen et al. (1999); Sambruna et al. (1997); Wolter et al. (1998) and Worrall et al. (1990). We also checked the NASA Extragalactic Database (NED) for other objects classified as BL Lacs/blazars, or that could be classified as such.

The total number of considered blazars is 268. Of these, 227 have been observed by *ROSAT* and 88 have spectral information in the 2–10 keV band [of these latter sources, 77 have both soft (*ROSAT*) and hard X–ray data]. The details about the breakdown of source among HBL/LBL/FSRQ, and of the data among different X–ray telescopes is reported in Table 2. The data obtained with *Einstein* have large errors associated and for almost all sources better *ROSAT* data were available. For these reasons, the Einstein data are not used to derive any of the results (or figures) of this paper.

Some sources have been observed many times either by the same and/or by different satellites. For these sources, we chose the observation with the best $\chi^2_{\rm r}$ in the analysis[2].

For the most "famous" sources, like 3C 273, Mkn 421, Mkn 501, PKS 2155–304, we do not include the results of all the observations made by all satellites, but we have only listed few representative data (those with the best $\chi^2_{\rm r}$) for each of these sources (typically, one spectral datum for each observing satellite).

Of course, the resulting catalogue is not a complete sample. Nevertheless, it is the largest database of its kind, and we think it is representative of the entire blazar class. The large number of sources in each sub–category of blazars guarantees a meaningful comparison between their X–ray properties, and their relation with the fluxes in other bands.

3.2. Format of the catalogue

Data are presented in Table 5 with the following format. For each source, Table 5 gives the IAU name, the redshift, the fluxes in the radio band (5 GHz), optical (V band) and X–ray (1 keV) and the X–ray photon spectral index. In the last columns of Table 5 we also indicate

[2] We have verified that this choice does not introduce a bias towards particularly faint states of the sources (for which lower statistics could yield larger error bars and better χ^2) nor towards particularly high states (for which a better statistics could yield lower values of the reduced χ^2 due to the increased number of degrees of freedom).

Table 2. Number of observations obtained from various satellites and number of observed blazars (divided into different subclasses). For the total number of sources we have excluded multiple observations by different satellites of the same source.

	No. oss.	HBL	LBL	FSRQ
ASCA	52	14	9	24
EXOSAT	33	16	7	10
BeppoSAX	47	29	9	8
ROSAT	227	129	54	44
EINSTEIN	62	7	23	32
TOTAL	421	136	63	69

to which subclass the blazar belongs to (1 for HBL, 2 for LBL and 3 for FSRQs) and the observing satellite (RO = *ROSAT*; AS = ASCA; EI = *Einstein*; EX = EXOSAT; SA = *Beppo*SAX).

For the radio fluxes we calculated the averaged value when there was more than one observation; the optical fluxes reported in the NED database are calculated using the indicated magnitude dereddened with the galactic extinction A_B as reported by the NED database. When in the literature we found only the 0.1–2.4 keV and/or the 2–10 keV integrated fluxes, we derived the monochromatic ones at 1 keV using the corresponding X–ray spectral index. All fluxes presented in Table 5 are not K–corrected.

To compute the luminosities, we used $H_0 = 50$ km s^{-1} Mpc^{-1} and $q_0 = 0.5$, and for the K–correction we assumed a radio spectral index $\alpha = 0$ for all sources; an optical spectral index $\alpha = 0.5$ for HBL and $\alpha = 1$ for the rest of the sources; for the X–ray data we used the listed X–ray spectral index. Also the broad band spectral indices have been K–corrected.

The K–correction for sources with unknown redshift was computed using the average redshift appropriate for each sub–class (i.e. $\langle z\rangle_{\rm HBL} = 0.249$, $\langle z\rangle_{\rm LBL} = 0.457$ and $\langle z\rangle_{\rm FSRQ} = 1.265$).

4. Results

Theoretical models that explain the nature of the observed behaviors of blazars predict a continuity between the various subclasses. To check if this is true for the objects belonging to our catalogue, we computed the distributions of redshifts, X–ray and broad band spectral indices and luminosities.

Moreover, another goal of this work is to compare the blazar characteristics observed in the soft and in the hard X–ray band. We divided our sources into two groups, one with the data obtained with *ROSAT* (0.1–2.4 keV) and another one with the data obtained with EXOSAT, ASCA, and *Beppo*SAX (2–10 keV). As anticipated (see Table 2) the first group of sources contains 227 objects, while the second one contains 88 sources (38 HBL, 19 LBL and 31 FSRQ). In addition, since the two sources 2344+514 and 1652+398 are very variable and we have data both

Table 3. Average values of X–ray spectral indices, redshifts, νL_ν luminosities in different bands and broad band spectral indices. The listed errors are weighted errors.

	HBL	LBL	FSRQ
$\alpha_{\rm x}$[2–10 keV]	1.34 ± 0.05	0.84 ± 0.07	0.65 ± 0.04
$\alpha_{\rm x}$[0.1–2.4 keV]	1.28 ± 0.04	1.39 ± 0.08	0.76 ± 0.06
z	0.25 ± 0.02	0.46 ± 0.05	1.27 ± 0.12
Log $\nu_{\rm r} L_{\nu_{\rm r}}$	41.51 ± 0.07	43.65 ± 0.16	44.93 ± 0.13
Log $\nu_{\rm o} L_{\nu_{\rm o}}$	44.66 ± 0.06	45.49 ± 0.12	46.35 ± 0.11
Log $\nu_{\rm x} L_{\nu_{\rm x}}$	44.62 ± 0.08	44.52 ± 0.15	45.89 ± 0.11
$\alpha_{\rm ro}$	0.36 ± 0.01	0.56 ± 0.02	0.66 ± 0.01
$\alpha_{\rm ox}$	1.03 ± 0.02	1.38 ± 0.02	1.21 ± 0.02
$\alpha_{\rm rx}$	0.59 ± 0.01	0.84 ± 0.01	0.85 ± 0.01

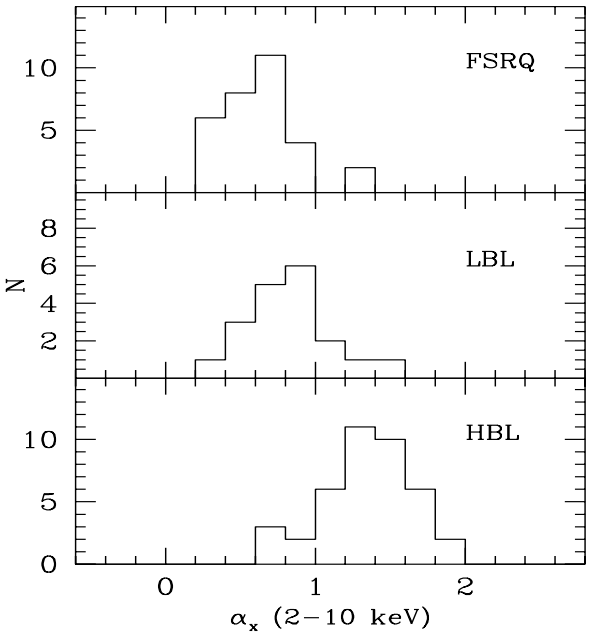

Fig. 1. Distribution of the energy spectral index $\alpha_{\rm x}$ in the 2–10 keV hard X–ray energy band. Note the difference between the HBL and the other two subclasses of blazars. The KS test gives a probability $P = 8 \times 10^{-6}$ that the HBL and the LBL values are drawn from the same distribution ($P = 2 \times 10^{-12}$ for HBL–FSRQ and $P = 0.03$ for LBL–FSRQ).

for a quiescent and a flaring state, in the latter group we put the data of two observations (one for the high and one for the low state) for each of them.

4.1. Histograms

The distribution of spectral indices, redshifts and luminosities are shown by the histograms in Figs. 1–9. In the figure captions we give the probability, according to the Kolmogorov–Smirnov (KS) test, that two distributions are drawn from the same parent population, comparing HBLs and LBLs, HBLs and FSRQs, LBLs and FSRQs.

The mean values of the plotted quantities are listed in Table 3.

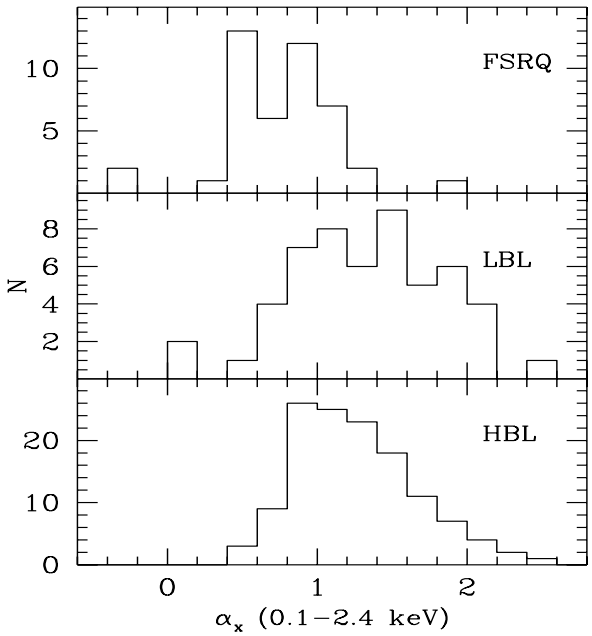

Fig. 2. Distribution of the energy spectral index $\alpha_{\rm x}$ in the 0.1–2.4 keV soft X–ray energy band. In this case LBL are more similar to HBL than to FSRQ. KS test results: $P = 0.20$ for HBL–LBL; 10^{-8} for HBL–FSRQ; 5×10^{-8} for LBL–FSRQ.

4.1.1. Spectral indices

The distributions of the energy spectral indices (Figs. 1 and 2) show that for FSRQ we have an average value less than unity in both energy ranges. This suggests that for this subclass of blazars we are observing only the inverse Compton component in the entire X–ray band, from 0.1 to 10 keV. For HBL, instead, the average energy spectral index is greater than unity, indicating that we are observing the synchrotron component after its peak. On average, LBL show a flattening going from the soft to the hard X–ray bands.

These results suggest that both the soft and the hard X–ray bands are dominated by the inverse Compton process in FSRQs and by the synchrotron process in HBL, while in LBL we have the synchrotron flux dominating in the soft band and the flatter Compton component emerging at higher X–ray energies.

4.1.2. Redshift

While the redshifts of FSRQs are quite uniformly distributed up to a value of $\simeq$3, BL Lacs have redshifts lower than 1 (and HBL have lower redshifts than LBL, see Fig. 3). There is no significant difference between the redshift distributions of sources observed in the hard and in the soft X–ray bands. Of the sources in our sample, about 25% have no measured redshift (38 HBL and 17 LBL). This incompletness, even if not severe, could bias the shown redshift distribution of HBLs towards the lower part (since larger redshifts are more difficult to measure).

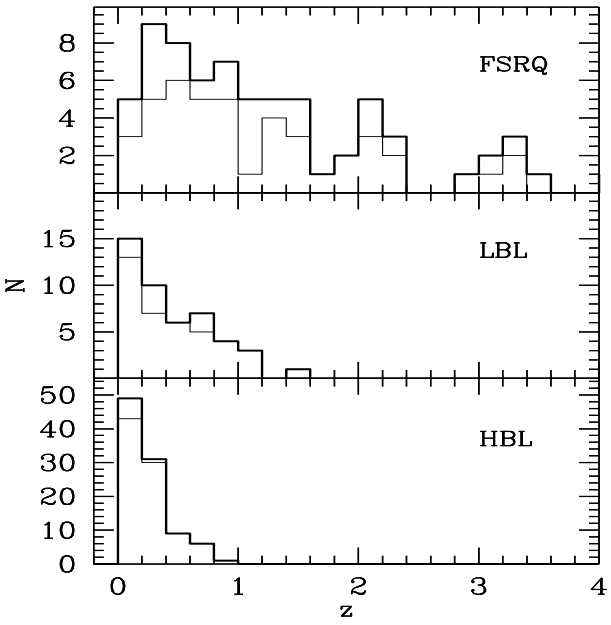

Fig. 3. Redshift distribution for the three subclasses. Thick solid lines refer to the entire sample, while thin solid lines refer to sources with only *ROSAT* data. KS test results (for the entire sample): $P = 2 \times 10^{-3}$ for HBL–LBL; 9×10^{-17} for HBL–FSRQ; 5×10^{-5} for LBL–FSRQ.

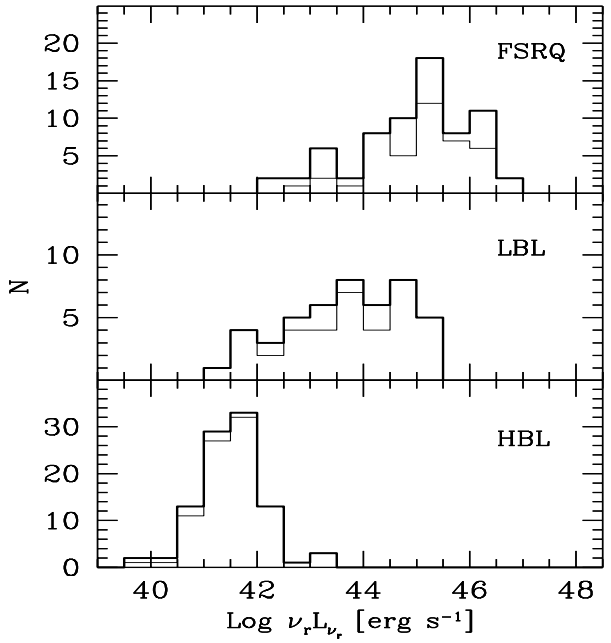

Fig. 4. Distribution of the radio luminosity for the three subclasses. Thick solid lines refer to the entire sample, while thin solid lines refer to sources with only *ROSAT* data. KS test results (for the entire sample): 7×10^{-19} for HBL–LBL; 7×10^{-33} for HBL–FSRQ; 10^{-6} for LBL–FSRQ.

4.1.3. Luminosities

From the radio, optical and 1 keV monochromatic fluxes we have calculated the "νL_ν" luminosities in the corresponding bands. The distributions of radio and optical luminosities (Figs. 4 and 5) show a continue variation in the three subclasses of blazar: HBLs are the least powerful sources, and FSRQs are the most luminous objects. this is more pronounced in the radio than in the optical band. The X–ray luminosities of HBLs and LBLs are very similar (Fig. 6), while FSRQs are more luminous by a factor of 10.

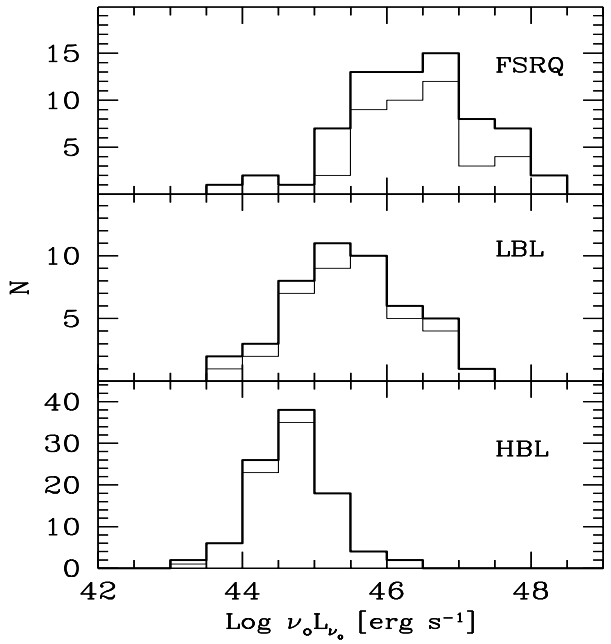

Fig. 5. Distribution of the optical luminosity for the three subclasses. Thick solid lines refer to the entire sample, while thin solid lines refer to sources with only *ROSAT* data. KS test results (for the entire sample): $P = 2 \times 10^{-7}$ for HBL–LBL; 10^{-22} for HBL–FSRQ; 3×10^{-5} for LBL–FSRQ.

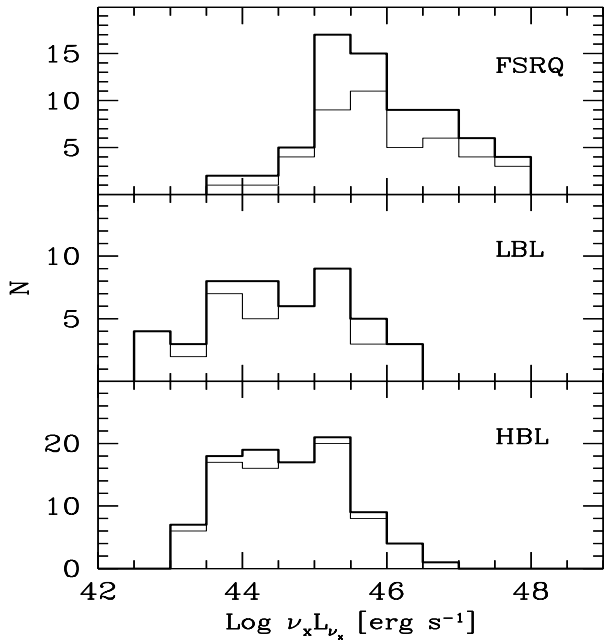

Fig. 6. Distribution of the X–ray luminosity for the three subclasses. Thick solid lines refer to the entire sample, while thin solid lines refer to sources with only *ROSAT* data. KS test results (for the entire sample): $P = 0.6$ for HBL–LBL; 3×10^{-13} for HBL–FSRQ; 2×10^{-8} for LBL–FSRQ.

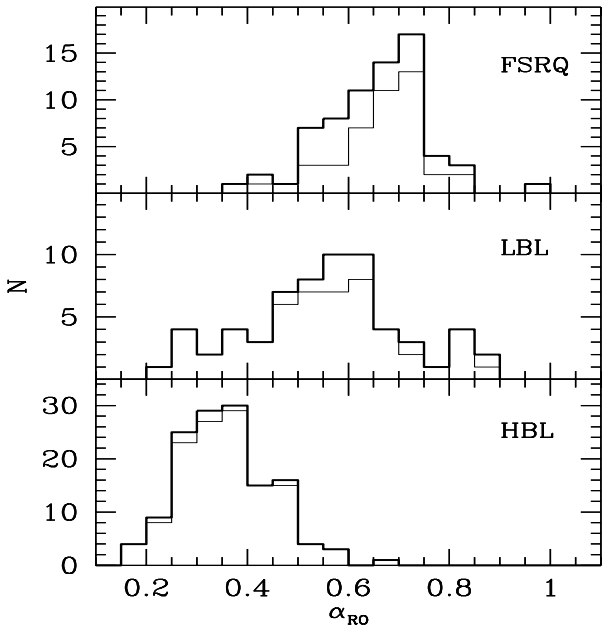

Fig. 7. Distribution of the broad band radio–optical spectral index for the three subclasses. Fluxes have been K–corrected as explained in the text. Thick solid lines refer to the entire sample, while thin solid lines refer to sources with only *ROSAT* data. KS test results (for the entire sample): $P = 4 \times 10^{-18}$ for HBL–LBL; 2×10^{-35} for HBL–FSRQ; 4×10^{-4} for LBL–FSRQ.

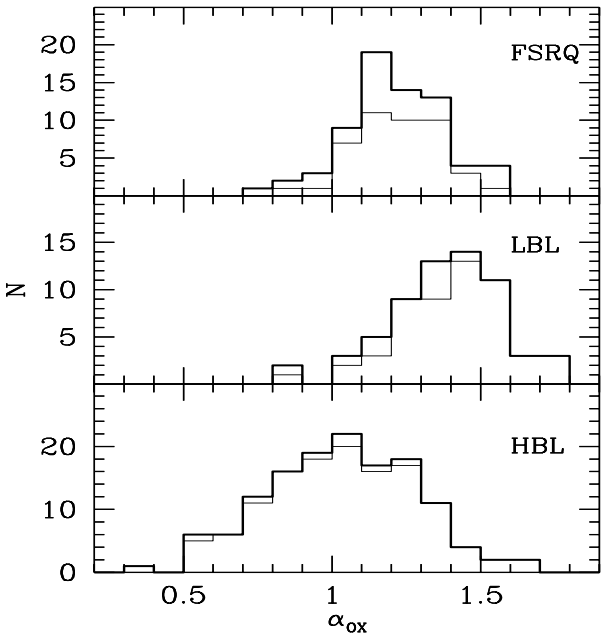

Fig. 8. Distribution of the broad band optical–X–ray spectral index for the three subclasses. Fluxes have been K–corrected as explained in the text. Thick solid lines refer to the entire sample, while thin solid lines refer to sources with only *ROSAT* data. KS test results (for the entire sample): $P = 5 \times 10^{-17}$ for HBL–LBL; 10^{-5} for HBL–FSRQ; 10^{-8} for LBL–FSRQ.

4.1.4. Broad band indices

Also the broad band spectral index $\alpha_{\rm ro}$ changes smoothly between the subclasses of blazar (Fig. 7). On average, it becomes steeper going from HBL to FSRQs. The optical to X–ray broad band index distribution (Fig. 8) is broader for HBL, with an average value smaller than for LBL and FSRQs. The spectral index $\alpha_{\rm rx}$ (Fig. 9) is on average the same for FSRQs and LBLs, and obviously flatter (by definition) for HBLs.

5. The average SED

In Fig. 10 we show the sequence of average SEDs as published by F98, but including the [2–10 keV] averages spectral indices and fluxes. The latter have been constructed considering only the same samples considered by F98.

It can be seen that in general the 2–10 keV fluxes and spectral indices connect smoothly on the softer *ROSAT* data even if they are, on average, flatter than the latter. This is due to the emergence, in the hard X–ray band, of the inverse Compton component which is progressively more dominant as the luminosity increases.

For the average SED corresponding to the second lowest luminosity bin, there is a mismatch between the soft and hard X–ray data. By comparing the data of each source in common, we found that all 5 sources were brighter when observed by ASCA or *Beppo*SAX than at the time of the *ROSAT* observations. We therefore believe that the mismatch is due to the variable nature of the objects and the small number of sources in this luminosity bin.

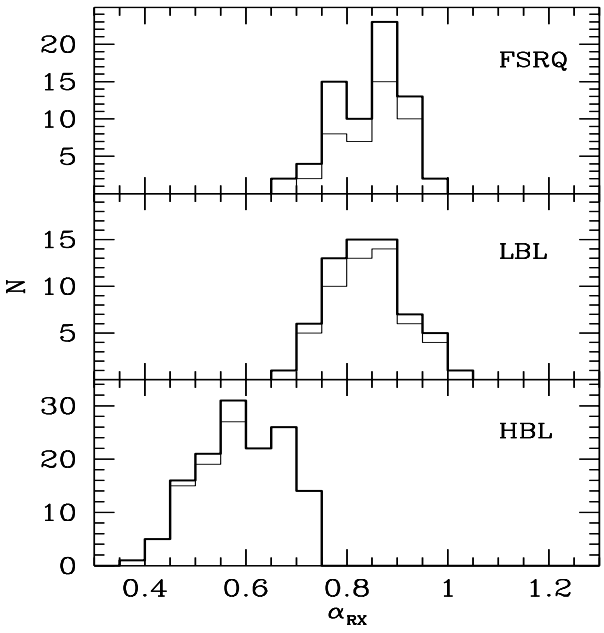

Fig. 9. Distribution of the broad band radio–X–ray spectral index for the three subclasses. Fluxes have been K–corrected as explained in the text. Thick solid lines refer to the entire sample, while thin solid lines refer to sources with only *ROSAT* data. KS test results (for the entire sample): $P = 8 \times 10^{-39}$ for HBL–LBL; 5×10^{-40} for HBL–FSRQ; 0.7 for LBL–FSRQ.

The average spectral indices of the objects in common with F98 are listed in Table 4, which also lists the average

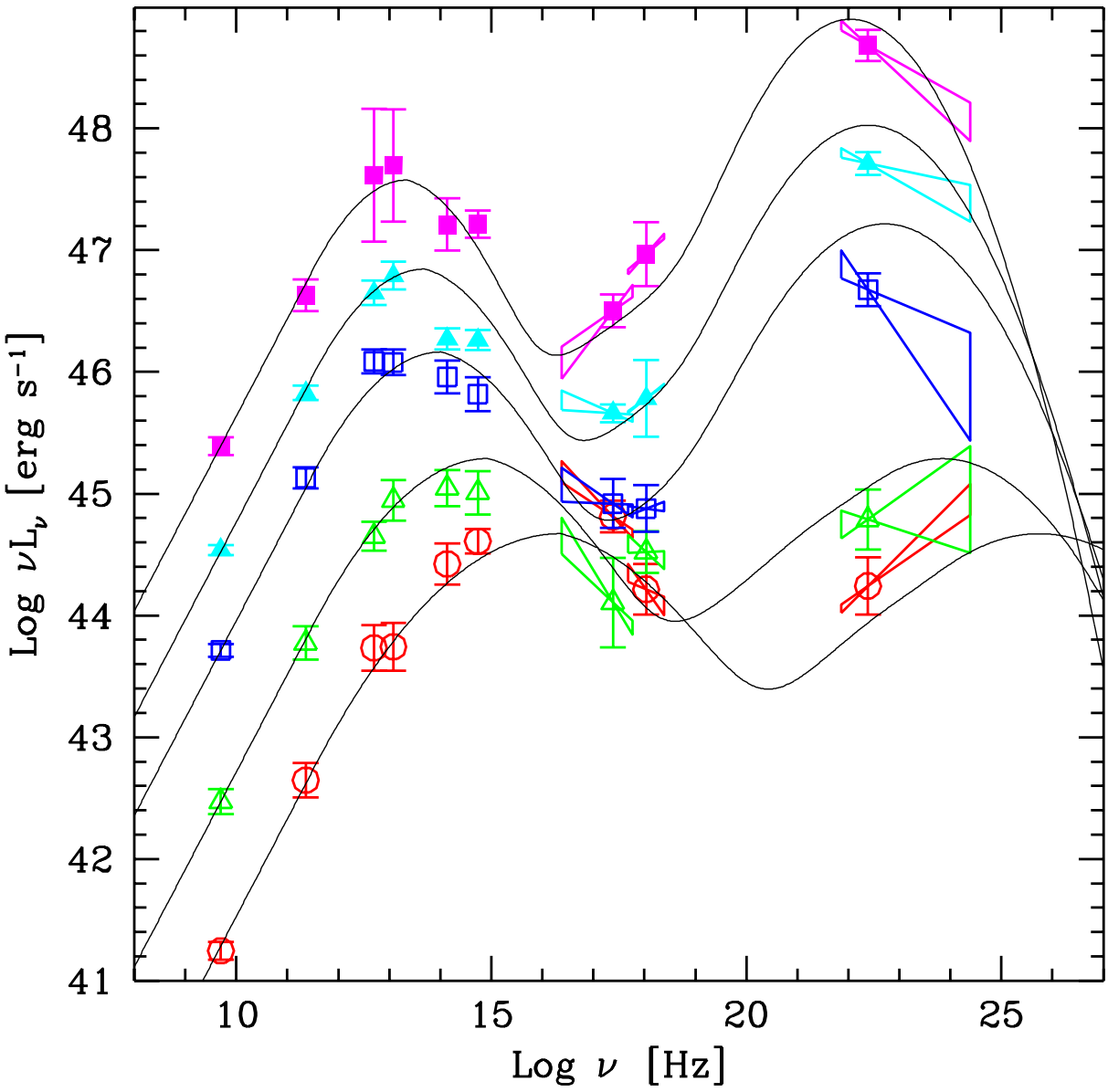

Fig. 10. The average SED of the blazars studied by Fossati et al. (1998), including the average values of the hard X–ray spectra. The thin solid lines are the spectra constructed following the parameterization proposed in this paper.

luminosities at 4.47 keV (the logarithmic mid point between 2 and 10 keV).

The continuous lines in Fig. 10 correspond to a simple parametric model derived by the one introduced by Fossati et al. (1998). We introduce minor modifications, adopted both to better represent our data at small luminosities and to follow a more physical scenario, in which the low power HBLs can be described by a pure synchrotron–self Compton model (see e.g. Ghisellini et al. 1998). We remind the reader here of the key assumptions of the F98 parametric model:

- The observed radio luminosity $L_{\rm R} = (\nu L_\nu)|_{5\ \rm GHz}$ is assumed to be linearly proportional to the bolometric luminosity, and related to the location of the synchrotron peak through:

$$\nu_{\rm s} \propto L_{\rm R}^{-\eta} \qquad (1)$$

Table 4. Average values of the X–ray luminosity at 4.47 keV (νL_ν values) and average 2–10 keV spectral indices, for the sources in common with Fossati et al. (1998), for each radio luminosity bin.

$< \log \nu_{\rm r} L_{\nu_{\rm r}} >$	$< \log \nu_{\rm x} L_{\nu_{\rm x}} >$ @4.47 keV	$N_{\rm sources}$	$\alpha_{\rm x}$ 2–10 keV
<42	44.2	12	1.39 ± 0.21
42–43	44.5	5	1.19 ± 0.21
43–44	44.9	6	0.95 ± 0.11
44–45	45.8	6	0.68 ± 0.02
>45	47.0	11	0.58 ± 0.06

where $\eta = 1.8$ for $L_{\rm R} < 3 \times 10^{42}$ erg s^{-1} and $\eta = 0.6$ for $L_{\rm R} > 3 \times 10^{42}$ erg s^{-1}.

- The ratio between the Compton and the synchrotron peak frequencies is constant: $\nu_c/\nu_s = 5 \times 10^8$ for all luminosities.
- The ratio between the power of the inverse Compton and the radio powers is constant: $L_c/L_R = 3 \times 10^3$ for all luminosities;
- The ratio between the radio and X–ray (at 1 keV) Compton luminosity is fixed.

The SED is then constructed assuming for the synchrotron component a flat ($\propto \nu^{-0.2}$) radio spectrum connecting to a parabola (in log–log space) peaking at ν_s. The junctions between the power law and the parabola is continuous. For the inverse Compton spectrum it is assumed that an initial power law of index $\alpha = 0.6$ ends in another parabola peaking at ν_c.

We modified the Fossati et al. (1998) description in the following way:

- We changed the values of η, assuming $\eta = 1.2$ and 0.4 for L_R smaller and greater than 10^{43} erg s^{-1};
- The ratio ν_c/ν_s is assumed to be constant with the same value as before for $L_R > 10^{43}$ erg s^{-1}, but for smaller radio luminosity we set:

$$\frac{\nu_c}{\nu_s} = 5 \times 10^8 L_{R,43}^{-0.4}; \quad (2)$$

- Below $L_R < 10^{43}$ erg s^{-1} we assume that the synchrotron and Compton peaks have the same luminosities. For greater L_R we assumed, as before, $L_c/L_R = 3 \times 10^3$.

The spectra predicted by this new parameterization are shown in Fig. 10 as thin solid lines. As anticipated, the assumptions described above have a physical motivation. In fact, for low luminosity sources, we have evidences that the seed photons producing the Compton spectrum are the locally produced synchrotron ones, with no or negligible contributions from seed photons produced externally to the jet (e.g. from the Broad Line Region). In this case:

i) The ratio ν_c/ν_s increases with ν_s as long as the scattering process is in the Thomson regime, and decreases with ν_s in the Klein Nishina regime;
ii) On average, the BL Lacertae objects detected by EGRET with $L_R < 10^{43}$ erg s^{-1} have roughly the same power in the synchrotron and Compton components;
iii) The radio luminosity $L_R = 10^{43}$ erg s^{-1} may corresponds to the power for which emission lines and/or external seed photons becomes important for the formation of the inverse Compton spectrum (see e.g. Ghisellini et al. 1998).

6. Correlations

In order to see if the proposed parameterization of the average SED of blazars (constructed on the basis of a subsample of the sources in our catalogue) can account for the general properties of all the blazars in our catalogue,

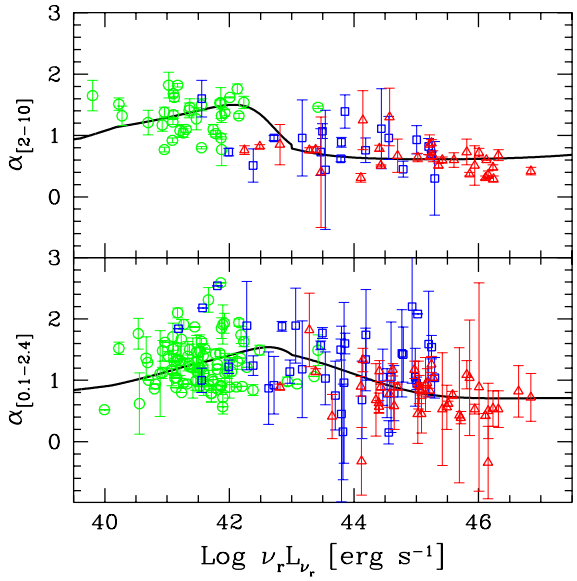

Fig. 11. Soft and hard X–ray spectral index vs. the radio luminosity. Circles: HBL, Squares: LBL, Triangles: FSRQs.

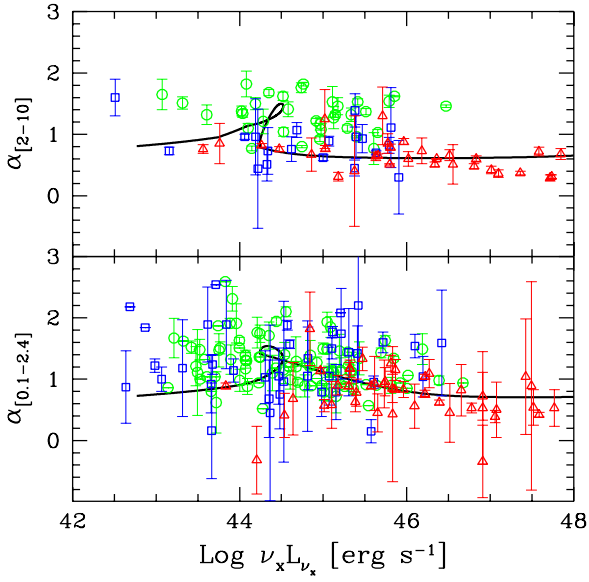

Fig. 12. Soft and hard X–ray spectral index vs. the X–ray luminosity. Circles: HBL, Squares: LBL, Triangles: FSRQs.

we have investigated the correlations between the X–ray spectral index (both hard and soft) with the radio and X–ray luminosities and with the broad band spectral indices. We have then considered the correlations between broad band indices. The results are shown in Figs. 12–18 (solid line), where we have superposed the relations predicted by the new parameterization.

In Figs. 11 and 12 we show the hard and soft X–ray indices as a function of the radio and X–ray luminosity for all sources, and compare these data with the model expectations. Note that the latter have been constructed to describe the *average* properties of blazars, whatever the scatter around it. Bearing this in mind, we can consider the description of the model quite satisfactorily.

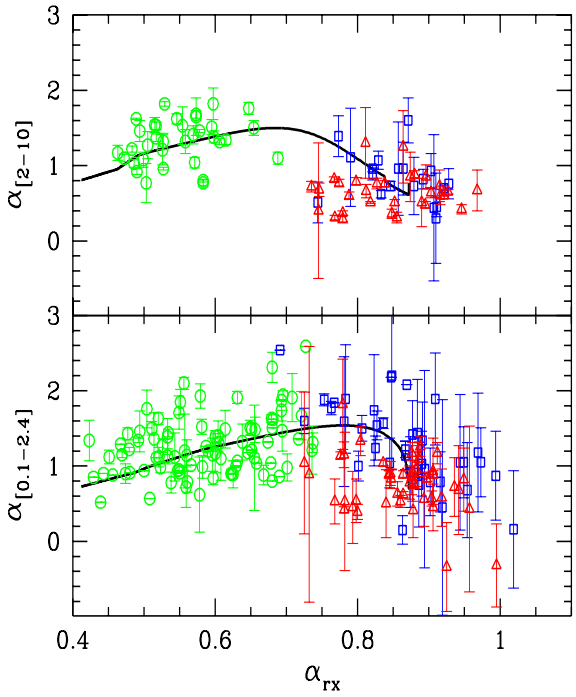

Fig. 13. Soft and hard X–ray spectral index vs. the broad band radio to X–ray index. Circles: HBL, Squares: LBL, Triangles: FSRQs.

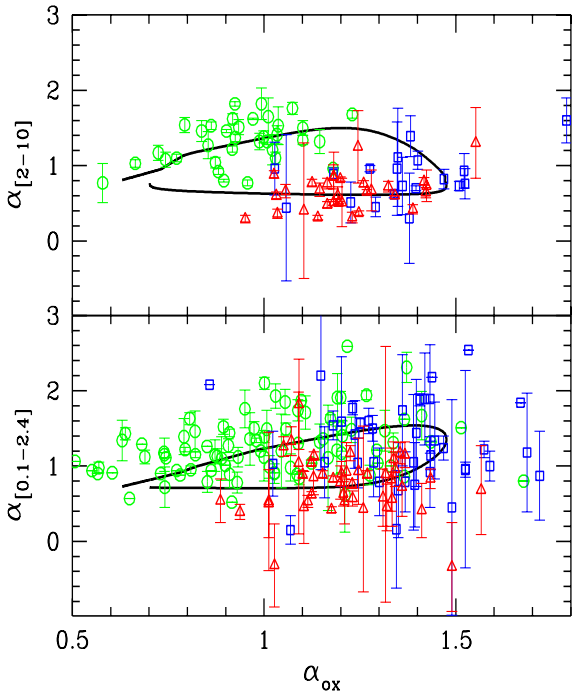

Fig. 15. Soft and hard X–ray spectral index vs. the broad band optical to X-ray index. Circles: HBL, Squares: LBL, Triangles: FSRQs.

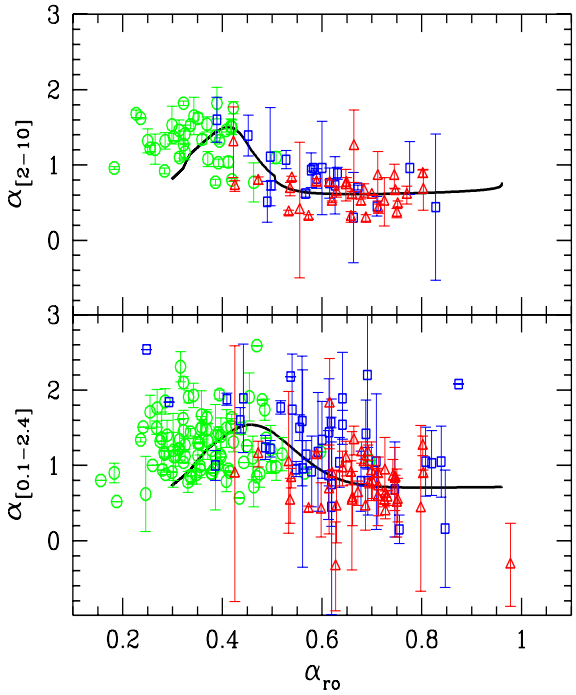

Fig. 14. Soft and hard X–ray spectral index vs. the broad band radio to optical index. Circles: HBL, Squares: LBL, Triangles: FSRQs.

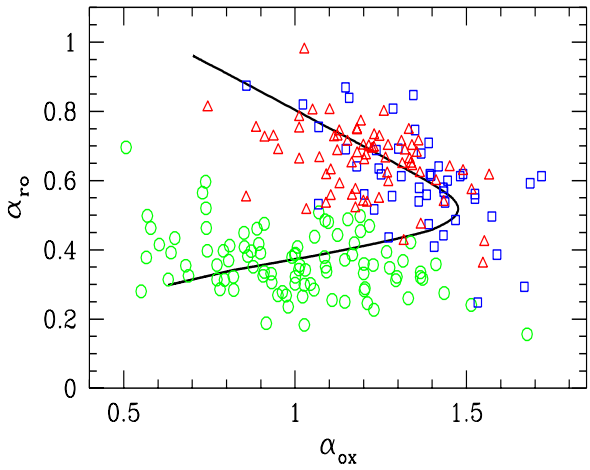

Fig. 16. Radio to optical vs. optical to X–ray broad band indices. Circles: HBL, Squares: LBL, Triangles: FSRQs.

In Fig. 13 we show the hard and soft X–ray indices as a function of the broad band index α_{rx}. The model well describes the small α_{rx} part (corresponding to HBLs), but fails to describe the X–ray flattest sources with the steeper value of α_{rx}. This is due to two reasons: i) the slope of the power law of the Compton component is assumed to be $\alpha = 0.7$, so that flatter indices are not possible; ii) the ratio between the radio and the 1 keV Compton luminosity is fixed for all sources. This results in a saturated value of $\alpha_{rx} \sim 0.85$, occurring when the Compton component dominates at 1 keV (i.e. for powerful sources).

In Figs. 14 and 15 we show α_X as a function of α_{ro} and α_{ox}: the average properties are well described by the model.

In Fig. 16, we show the "classic" α_{ro}–α_{ox} diagram for the two subsamples of sources. Note that the model well describes all the data but those sources with the largest

Table 6. References used in Table 5. TW means This Work.

Ba94:	Bade et al. (1994)	Gh99:	Ghisellini et al. (1999)	Pa95:	Padovani et al. (1995)
Ba98:	Bade et al. (1998)	BSGh:	Ghisellini in BeppoSAX Archive	Pa99:	Padovani et al. (1999)
Br85:	Bregman et al. (1985)	Gi98:	Giommi et al. (1998)	Pe96:	Perlman et al. (1996)
Br94:	Brinkmann et al. (1994)	Gi99:	Giommi et al. (1999)	Sa94:	Sambruna et al. (1994)
Br97:	Brinkmann et al. (1997)	Go95:	Ghosh et al. (1995)	Sa97a:	Sambruna et al. (1997)
Ca97:	Cappi et al. (1997)	Gr96:	Greiner et al. (1996)	Sa97b:	Sambruna et al. (1997)
Co95:	Comastri et al. (1995)	Kh81:	Khuer et al. (1981)	Sa99:	Sambruna et al. (1999)
Co97:	Comastri et al. (1997)	Ku98:	Kubo et al. (1998)	Sb96:	Siebert et al. (1996)
Cs00:	Costamante et al. (2000)	IT90:	Impey et al. (1990)	Sb99:	Siebert et al. (1999)
El99:	Elvis et al. (1999)	IT91:	Impey et al. (1991)	Sn97:	Sing et al. (1997)
Fa97:	Fabian et al. (1997)	La96:	Lamer et al. (1996)	Ta00:	Tagliaferri et al. (2000)
Fa98:	Fabian et al. (1998)	Le97:	Leighly et al. (1997)	Tv99:	Tavecchio et al. (2000)
Fo98:	Fossati et al. (1998)	LM99:	Laurent-Muehleisen et al. (1999)	VV93:	Veron-Cetty et al. (1993)
Fo98b:	Fossati et al. (1998)	Ma98b:	Maraschi et al. (1998)	Xu99:	Xue et al. (1999)
Ge96:	George et al. (1996)	BSMc:	Maccacaro in BeppoSAX Archive	Ya98:	Yaqoob et al. (1998)
Gh93:	Ghisellini et al. (1993)	Na96:	Nass et al. (1996)	Wa99:	Watson et al. (1999)
Gh98:	Ghisellini (1998)	NED:	NASA-IPAC Extragalactic Database	Wo98:	Wolter et al. (1998)
Gh98b:	Ghisellini et al. (1998)	Or98:	Orr et al. (1998)	Wo90:	Worrall et al. (1990)

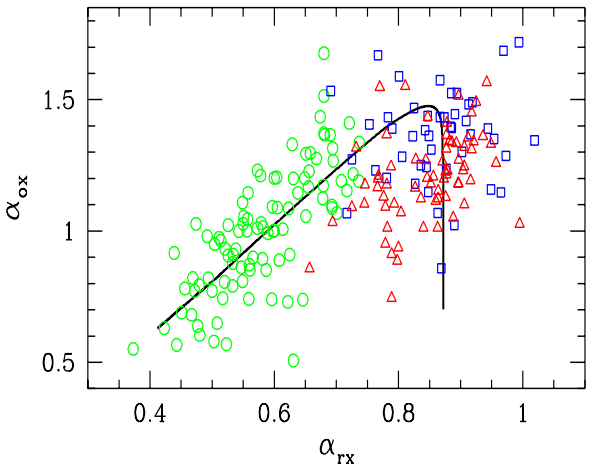

Fig. 17. Optical to X–ray vs. radio to X–ray broad band indices. Circles: HBL, Squares: LBL, Triangles: FSRQs.

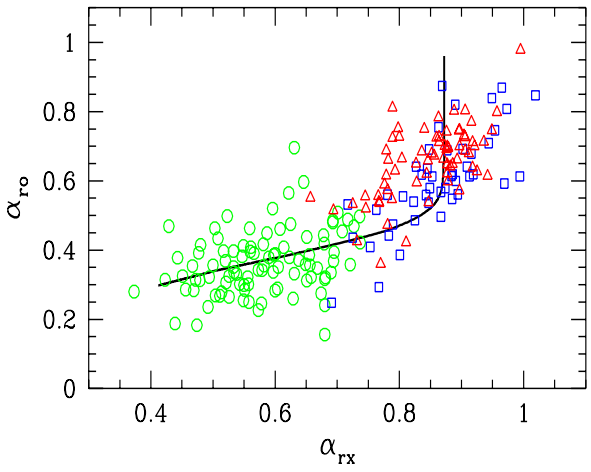

Fig. 18. Radio to optical vs. radio to X–ray broad band indices. Circles: HBL, Squares: LBL, Triangles: FSRQs.

values of α_{ox}, corresponding to "transition" sources between the LBLs and FSRQ.

Figures 17, and 18: note that HBL are well separated from the other classes of blazars. Note also that the model, by construction, has an asymptotic limit for α_{rx}, whose value therefore saturates at $\alpha_{rx} \simeq 0.85$.

7. Discussion

The large database of X–ray spectra of blazars we have collected has allowed to test the blazar sequence scheme aiming to unify the different behaviors of blazars on the basis of a single parameter, i.e. the bolometric observed luminosity. We have found that the proposed parameterization can account for the average properties of the blazars in our sample, even if the scatter around the predicted average quantities is sometimes large.

We confirm, on a statistical basis, that more powerful blazars emit the X–rays by the inverse Compton process, while in less powerful objects the dominant mechanism is synchrotron, and the transition is smooth, with LBL possibly showing both contributions.

The Fossati et al. (1998) parameterization scheme to reproduce the blazar SED is able to fit also our new hard

X–ray data and the correlations between broad band indices of the sources in our sample. However, we propose to slightly change this parameterization especially for the low power objects (i.e. the HBLs), in line with the idea that HBLs are characterized by a pure synchrotron self–Compton spectrum, without extra contributions produced by non locally produced seed photons.

In this paper, and in Fossati et al. (1998), the power law relation between the synchrotron peak frequency and the radio luminosity changes slope at some critical radio power, of the order of 3–10 $\times$ 10^{42} erg s^{-1}. This agrees with the absence of broad emission lines in these objects. It has still to be proven, however, if the non visibility of emission lines in low power objects is due to a genuine lack of emitting clouds, or is due to a weak ionizing continuum. If the latter hypothesis is true, then we expect that the broad line region indeed exists, but at smaller radii than in more powerful objects. In this case, the lack of the external Compton component is not due to the lack of external photons, but possibly to the fact that the dissipation region in these sources is beyond the broad line region: in this case the corresponding energy density of line photons is seen, in the comoving frame of the blob, depressed by the square of the bulk Lorentz factor.

Acknowledgements. We thank the anonimous referee for useful suggestions and Luigi Costamante for discussions. This research made use of the NASA/IPAC Extragalactic Database (NED) which is operated by the Jet Propulsion Laboratory, Caltech, under contract with the National Aeronautics and Space Administration. We acknowledge finantial support from the MURST.

References

Bade, N., Fink, H. H., & Engels, D. 1994, A&A, 286, 381
Bade, N., Beckmann, V., Douglas, N. G., et al. 1998, A&A, 334, 459
Bregman, J. N., Glassgold, A. E., Huggins, P. J., & Kinney, A. L. 1985, ApJ, 291, 505
Brinkmann, W., & Siebert, J. 1994, A&A, 285, 812
Brinkmann, W., Siebert, J., Feigelson, E. D., et al. 1997, A&A, 323, 739
Cappi, M., Matsuoka, M., Comastri, A., et al. 1997, ApJ, 478, 492
Comastri, A., Molendi, S., & Ghisellini, G. 1995, MNRAS, 277, 297
Comastri, A., Fossati, G., Ghisellini, G., & Molendi, S. 1997, ApJ, 480, 534
Costamante, L., Ghisellini, G., Giommi, P., et al. 2000, in X–ray '99: Stellar Endpoints, AGN and the Diffuse Background, in press [astro-ph/0001410]
Danly, L., Lockman, F. J., Meade, M. R., & Savage, B. D. 1992, ApJS, 81, 125
Dickey, J. M., & Lockman, F. J. 1990, ARA&A, 28, 215
Elvis, M., Lockman, F. J., & Wilkes, B. J. 1989, AJ, 97, 777
Elvis, M., Fiore, F., Siemiginowska, A., et al. 1999, HEAD, 31, 2305
Fabian, A. C., Brandt, W. N., McMahon, R. G., & Hook, I. M. 1997, MNRAS, 291, L5
Fabian, A. C., Iwasawa, K., McMahon, R. G., et al. 1998, MNRAS, 295, L25
Fossati, G., Celotti, A., Ghisellini, G., & Maraschi, L. 1997, MNRAS, 289, 136
Fossati, G., Maraschi, L., Celotti, A., Comastri, A., & Ghisellini, G. 1998, MNRAS, 299, 433
Fossati, G., Chiappetti, L., Celotti, A., et al. 1998, Nuclear Physics B (p.s.) 69/1–3, 423
George, I. M., & Turner, T. J. 1996, ApJ, 461, 198
Ghisellini, G., Padovani, P., Celotti, A., & Maraschi, L. 1993, ApJ, 407, 65
Ghisellini, G., & Madau, P. 1996, MNRAS, 280, 67
Ghisellini, G. 1998, Nuclear Physics B (p.s.) 69/1–3, 397
Ghisellini, G., Tagliaferri, G., Costamante, L., et al. 1998, Nuclear Physics B (p.s.) 69/1–3, 427
Ghisellini, G., Tagliaferri, G., & Giommi, P. 1999, IAUC, 7116
Giommi, P., Padovani, P., & Perlman, E. 1998, Nuclear Physics B (p.s.) 69/1–3, 407
Giommi, P., Fiore, F., Guainazzi, M., et al. 1998, A&A, 333, L5
Giommi, P., Massaro, E., Chiappetti, L., et al. 1999, A&A, 351, 59
Ghosh, K. K., & Soundararajaperumal, S. 1995, ApJS, 100, 37
Greiner, J., Danner, R., Bade, N., et al. 1996, A&A, 310, 384
Kellermann, K. I., Sramek, R., Schmidt, M., Shaffer, D. B., & Green, R. 1989, AJ, 98, 1195
Khuer, H., Witzel, A., Pauliny-Toth, I. I. K., & Nauber, U. 1981, A&AS, 45, 367
Kubo, H., Takahashi, T., Madejski, G., et al. 1998, ApJ, 504, 693
Impey, C.D., & Tapia, S. 1990, ApJ, 354, 124
Impey, C. D., Lawrence, C. R., & Tapia, S. 1991, ApJ, 375, 46
Lamer, G., Brunner, H., & Staubert, R. 1996, A&A, 311, 384
Leighly, K. M., O'Brien, P. T., Edelson, R., et al. 1997, ApJ, 483, 767
Laurent–Muehleisen, S. A., Kollgaard, R. I., Ryan, P. J., et al. 1997, A&AS, 122, 235
Laurent–Muehleisen, S. A., Kollgaard, R. I., Feigelson, E. D., Brinkmann, W., & Siebert, J. 1999, ApJ, 525, 127
Lockman, F. J., & Savage, B. D. 1995, ApJS, 97, 1
Mannheim, K. 1993, A&A, 269, 67
Maraschi, L., Ghisellini, G., & Celotti, A. 1992, ApJ, 397L, 5
Maraschi, L., Celotti, A., Fossati, G., et al. 1998, Nuclear Physics B (p.s.) 69/1–3, 453
Murphy, E. M., Lockman, F. J., Laor, A., & Elvis, M. 1996, ApJS, 105, 36
Nass, P., Bade, N., Kollgaard, R. I., et al. 1996, A&A, 309, 419
Orr, A., Yaqoob, T., Parmar, A. N., et al. 1998, A&A, 337, 685
Padovani, P., & Giommi, P. 1995, MNRAS, 277, 1477
Padovani, P., Morganti, R., Siebert, J., et al. 1999, MNRAS, 304, 829
Perlman, E. S., Stocke, J. T., Wang, Q. D., & Morris, S. L. 1996, ApJ, 456, 451
Reeves, J. N., Turner, M. J. L., Ohashi, T., & Kii, T. 1997, MNRAS, 292, 468
Sambruna, R. M., Barr, P., Giommi, P., et al. 1994, ApJS, 95, 371
Sambruna, R. M., George, I. M., Madejski, G., et al. 1997, ApJ, 483, 774
Sambruna, R. M. 1997, ApJ, 487, 536

Sambruna, R. M., Ghisellini, G., Hooper, E., et al. 1999, ApJ, 515, 140
Sambruna, R. M., Chou, L. L., & Urry, C. M. 2000, ApJ, 533, 650
Siebert, J., Matsuoka, M., Brinkmann, W., et al. 1996, A&A, 307, 8
Siebert, J., Brinkmann, W., Gliozzi, M., Laurent–Muehleisen, S. A., & Matsuoka, M. 1999, AN, 320, 315
Sikora, M., Begelman, M. C., & Rees, M. J. 1994, ApJ, 421, 153
Sing, K. P., Shrader, C. R., & George, I. M. 1997, ApJ, 491, 515
Tagliaferri, G., Ghisellini, G., Giommi, P., et al. 2000, A&A, 354, 431
Tanaka, Y., et al. 1994, PASJ, 46, L37
Tavecchio, F., Maraschi, L., Ghisellini, G., et al. 2000, ApJ, in press [astro-ph/0003019]
Veron-Cetty, M. P., & Veron, P. 1993, ESO Scientific Report, Garching
Xue, S. J., & Zhang, Y. H. 2000, in X–ray '99: Stellar Endpoints, AGN and the Diffuse Background, in press [astro-ph/9911293]
Yaqoob, T., George, I. M., Turner, T. J., et al. 1998, ApJ, 505, L87
Watson, D., Hanlon, L., McBreen, D., et al. 1999, A&A, 345, 414
Wolter, A., Comastri, A., Ghisellini, G., et al. 1998, A&A, 335, 899
Worrall, D. M., & Wilkes, B. J. 1990, ApJ, 360, 396